

The Smithinator: Recumbent Vehicle Design and Entry for the 2020 ASME Human-Powered Vehicle Challenge

A Technical Report Submitted to the Department of Mechanical and Aerospace Engineering

Faculty of the School of Engineering and Applied Science
University of Virginia • Charlottesville, Virginia

In Partial Fulfillment of the Requirements of the Degree
Bachelor of Science, School of Engineering

Spring, 2020


Technical Project Team Members:

Todd Baber
Sandesh Banskota
Ethan Blundin
Ross Bonnin
Chloe Chang

Thomas DeAngelis
Michael Jeong
Yasmin Khanan
Jeanluc Lapierre
Brad Mahaffey

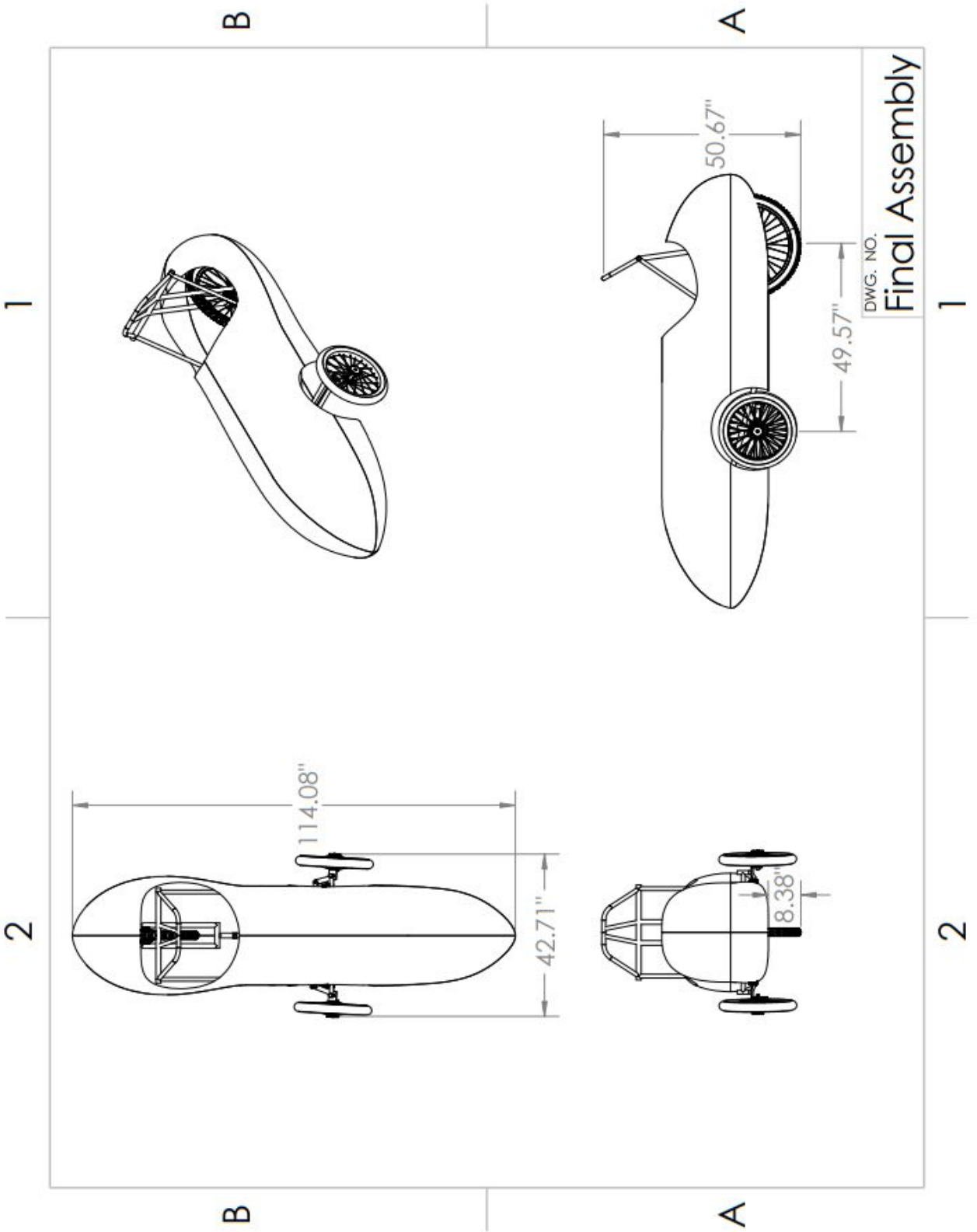
Coke Matthews
Jesse Patterson
Henry Qi
Kristin Schmidt

On my honor as a University Student, I have neither given nor received
unauthorized aid on this assignment as defined by the Honor Guidelines
for Thesis-Related Assignments

Signature  Date 4/27/2020

Approved  Date 21 Apr 2020
Natasha Smith, Department of Mechanical and Aerospace Engineering

3 VIEW DRAWING



Abstract

Bicycling as a form of transportation is a healthy, sustainable means of moving around. As it currently stands, the transportation sector in the United States, largely dominated by cars, contributes a substantial amount of pollution into the air and creates a strong consumer dependency on non-renewable resources, such as oil. With the Smithinator, the University of Virginia Human-Powered Vehicle Orange Team has sought to conceive a practical alternative to environmentally damaging vehicles by prioritizing consumer-friendliness, safety, and durability throughout the design.

A three-wheeled (tadpole configuration) recumbent vehicle was selected to provide an ideal balance of stability, speed, and ease of riding. In comparison to the standard upright bike, the recumbent tricycle reduces stresses on the rider's joints and provides back support, allowing a greater range of riders to feel comfortable. Furthermore, the design features an adjustable chain tensioner system to fit riders between 5'4" to 6'3".

The vehicle's full fairing features an open cockpit shape, which reduces the drag force by 36.5% compared to a fully closed fairing based on CFD simulations. The addition of a fairing to the Smithinator improves speed and ease of ride, as well as improving the rider's safety by reducing the effects of debris and inclement weather. The carbon-fiber material creates this aerodynamic advantage without adding substantial weight to the vehicle. Moreover, the under-seat Ackerman steering geometry is utilized to avoid tire slippage, while providing a reliable means of steering the vehicle.

Throughout the design process, the team utilized computer simulation software, such as SolidWorks, to analyze the structural, aerodynamic, and handling integrity. Moving into the manufacturing phase, the team iterated the design to fit real-world constraints. The team plans to continue developmental testing and consequent design iterations until the competition to ensure the vehicle is strong and safe.

Table of Contents

3-View Drawings	
Abstract	i
Table of Contents	ii
List of Figures	iv
List of Tables	v
1. Design	1
1.1 Objective	
1.2 New Design	
1.3 Team Design Strategy	
1.4 Background	
1.5 Prior Work	
1.6 Organizational Timeline	
1.7 Product Design Specifications	
1.8 Concept Development and Selection Methods	
1.8.1 Frame and Fairing Design	
1.8.2 Component Selection	
1.8.3 Safety and Electrical System	
1.8.4 Environmental Design Considerations	
1.9 Design Description	
2. Analysis	14
2.1 RPS Analyses	
2.1.1 Objectives, Methods, Assumptions	
2.1.2 Top Load Analysis	
2.1.3 Side Load Analysis	
2.2 Structural Analyses	
2.2.1 Rider Weight and Pedal Box Analysis	
2.2.2 Seat Analysis	
2.3 Aerodynamic Analyses	
2.3.1 Objectives, Methods, and Assumptions	
2.3.2 Results and Conclusions	
2.4 Cost Analyses	
2.5 Other Analyses	
2.5.1 Ackerman and Turning Radius Analysis	
2.5.2 Drivetrain Gearing Analysis	
2.5.3 Center of Mass Analysis	
2.5.4 Product Lifecycle / CO2 Analysis	
3. Testing	22
3.1 RPS Testing	
3.2 Developmental Testing	

3.2.1 Biomechanics Testing	
3.2.2 Seat Development Testing	
3.2.3 Weld Development Testing	
3.3 <i>Performance Testing</i>	
4. Safety	24
5. Conclusion	26
5.1 <i>Comparison</i>	
5.2 <i>Evaluation</i>	
5.3 <i>Recommendations</i>	
6. References	
7. Appendices	

List of Figures

1.1	Market analysis survey results	2
1.2	Frame geometries from previous design reports	2
1.3	Frame design iterations	7
1.4	Heat treated and molded foam	8
1.5	Fairing design enclosing RPS	8
1.6	Fairing design exposing RPS	8
1.7	Final fairing design	9
1.8	Chain gobbler on a tadpole trike	9
1.9	Initial seat design	10
1.10	Seat integrated into frame design	11
1.11	Steering mechanisms	12
1.12	Swivel angle and clearance	13
1.13	Caster angle diagram	13
1.14	Electrical architecture to control and power vehicle lights	13
1.15	Full assembly of vehicle	14
2.1	Top loading displacement with ASME specifications	15
2.2	Side loading displacement with ASME specifications	15
2.3	Pedal box FOS with ASME specifications	16
2.4	Rider weight simulation FOS using point load	16
2.5	Analysis of bottom seat deflection when integrated into frame	17
2.6	Boundary conditions of CFD analysis	17
2.7	CFD results of selected design from the side view	18
2.8	Ackerman top view	19
2.9	Power output based on drag coefficient and weight	21
3.1	Trochanter to Floor Distance	23
3.2	Biodex setup (40° angle at 100% TF distance shown)	23
3.3	Biodex Testing Mean Torque Output Across All Riders	24

List of Tables

I	Design Schedule for Fall Semester	4
II	Manufacturing and Testing Schedule for Spring Semester	4
III	2020 ASME Design Specifications	5
IV	UVA 2020 Self-Imposed Additional Specifications	5
V	Frame Decision Matrix	6
VI	Fairing Decision Matrix	7
VII	Steering Design Decision Matrix	12
VIII	Cost Breakdown by Subteam	19
IX	Ackerman Steering Geometry Analysis	20
X	Power Output and Speeds for 42T-34T Front Chainrings	21
XI	Total Life Cycle CO ₂ Emissions	22
XII	Emissions Conversions from Material Processes	22
XIII	Emissions Conversions from Electricity Usage	22
XIV	Biodex Testing Matrix	23
XV	Comparison of Self-Imposed Specifications and Analytical Results	26

1. Design

1.1 Objective

The mission of the American Society of Mechanical Engineers' (ASME) Human-Powered Vehicle Competition (HPVC) is to provide "...an opportunity for students to demonstrate the application of sound engineering design principles in the development of sustainable and practical transportation alternatives... to design and build efficient, highly engineered vehicles for everyday use--from commuting to work, to carrying goods to market." For this reason, the Orange Team at the University of Virginia sought to value these ideals in their vehicle specifications. The team aimed to design a vehicle that exemplifies the qualities of safety, sustainability, user-friendliness, and speed. The goal is to build a competitive vehicle, in terms of speed and endurance, while remaining practical for real-world scenarios.

1.2 New Design

The Smithinator is a new Human-Powered Vehicle, designed, manufactured, and tested exclusively by the UVA HPVC Orange Team during the 2019-2020 academic year. To the knowledge of the current team, UVA has never competed in an HPVC. The team also managed the administrative tasks of forming a new club, procuring funding, and arranging travel logistics.

1.3 Team Design Strategy

The 2020 UVA HPVC Orange and Blue teams originally started as one group of 27 students to brainstorm design ideas and collaborate on background research. Each member read three unique design reports from the HPVC Design Report archive, summarized findings, then developed concept designs in small groups. The team was exposed to a total of 81 design reports. These concept designs focused on presenting features and specifications that students wanted to see in the final design such as the top speed and frame design. After splitting into Orange and Blue teams based on design preferences, the Orange team used Shigley's 6-step design process to move forward from an identified need and problem statement to a final design (Shigley, 2011).

The UVA HPVC Orange Team was formed with a joint vision of a recumbent tadpole trike design. Team members were divided into six subteams - Frame, Fairing, Steering/Braking, Drivetrain/Biomechanics, Innovation, and Safety. The team lead and subteam leads were chosen and each subteam worked on tasks specific to their area and constantly communicated with other subteams to ensure synergy between the systems. Subteams presented weekly to their faculty advisor and received feedback on design progress. Each team member passed the SolidWorks Associate Certification Exam to demonstrate proficiency in CAD software.

1.4 Background

To support the team's goal to maximize user-friendliness, the team created a survey with questions about biking and transportation methods, in general, to better understand and incorporate consumer ideas into the design. The survey was dispersed to other groups team members were involved in, as well as sent out to local bike shops to share and posted to several Facebook and Reddit groups. From Fig. 1.1, the survey results indicate that the general consumer is mainly concerned with vehicle comfort and cost, less so for its speed and sustainability.

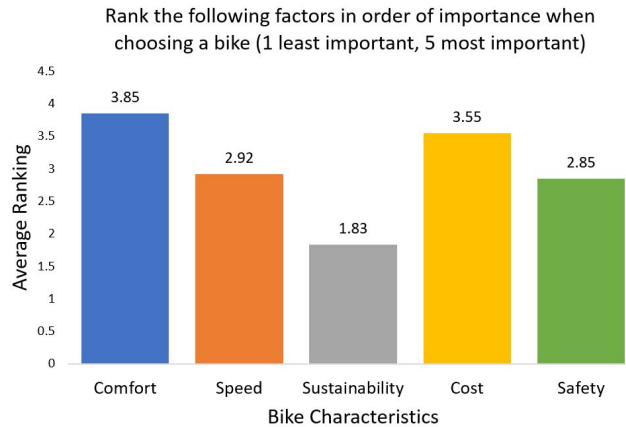


Fig. 1.1. Market Analysis Survey responses (from 242 respondents)

The team used bikes@Vienna, a recumbent bike shop in northern Virginia, as one of the main resources to inform design decisions throughout the entire design and manufacturing process. Team members visited the shop to get a feel for recumbent bicycles and ask shop workers questions about select components. Photos from these visits were used to understand how parts connect together, such as the implementation of the steering system.

Safety is also a major point of consideration in the design, and thus, the team considered safety accessories, as well as the structural integrity of the vehicle. Studies have shown that bicycle lights can reduce accident rates by up to 50% (Gulley, 2019). The team researched headlight, brake light, and sidelight implementation to improve safety while ensuring that the battery used to power the circuit complied with the ASME HPVC rules. This level of attention was also maintained while selecting the harness and other safety features. A majority of the safety rules came from the ASME HPVC handbook and their corresponding attachments were researched on Amazon to ensure their product descriptions complied with the rule book.

To ensure the vehicle was constructed with crash safety at the forefront, the team looked to reduce any areas of structural weakness. Consequently, the number of welds in the design was limited by utilizing pipe bending techniques. The frame geometry was modified from archived HPVC design reports from other universities, such as the designs from Pittsburgh, California State Northridge, and the University of Akron (Fig. 1.2). These vehicles had achieved high levels of success in their performance, their design reports, or both. Further, in the article, *Golden Rules of Trike Design*, Fenner recommends that the center of mass for a tadpole trike including the rider be in the front half of the wheelbase for stability at high speeds (Fenner, 2010).



Fig. 1.2. Frame geometries from previous design reports.

In the consideration of the steering system, the team considered over-seat, direct and indirect under-seat, and tilt steering. The turning radius and its relation to wheelbase and track were investigated, as it would end up dictating much of the overall design, as well as provide the vehicle with a favorable 12 foot turning radius. Ackermann, parallel, and anti-Ackermann steering systems were analyzed and compared to avoid skidding while turning. Multiple previous ASME HPVC designs, primarily the Ohio State Lynx, and commercial recumbent models, specifically Catrike and TerraTrike, were also studied to formulate decisions on the steering design. Over-seat and under-seat steering are the two main methods for steering. Over-seat steering mirrors driving a car, which is easier for new drivers to get accustomed to. However, over-seat steering is difficult to design for a tadpole recumbent bike. Direct, indirect, and tilt steering are methods of under-seat steering, and each brings different challenges and benefits. Tilt steering incorporates the entire frame of the bike, which can allow intuitive steering, but can be difficult to manufacture. Direct steering is the simplest to manufacture but becomes sensitive and twitchy at speeds greater than 30 mph. Indirect falls between the previous two in ease of manufacture and user-friendliness.

Additionally, the team conducted a literature review to understand the best position for the seat on the trike for riders to output maximum power to achieve optimal comfort and speed. The riders' patella should be horizontally inline with the end of the crank when the pedal is at 90° (Burke, 2003; Gregor et al., 2002). The seat recline angle should be between 30-75° (Too, 1993) and the seat to pedal distance should be 100% - 112% of the inner leg length from the ischium to the ground (Shennum, 1976; Too, 1993). To determine which exact position is best, the team consulted Dr. Shawn Russell in the UVA Motion Analysis and Motor Performance lab. Dr. Russell helped develop a biomechanics testing procedure to test rider physical abilities without a completed vehicle. The results from this study along with theoretical calculations developed by the team (section 2.5.2) were used to estimate the required power output for team design choices.

Goro Tamai's *The Leading Edge* was consulted for fairing background research on basic aerodynamic principles. The team came across cost-effective fairings made from foam in past design reports and decided to look into doing something similar. Foam samples of varying densities were obtained from Worldwide Foam on which the team performed tests to determine its feasibility as fairing material. These tests are expanded on further later in the report. The team also conducted wet-layup tests to learn the basics of designing and working with carbon fiber.

The team also determined that rider workouts were needed to condition riders for high performance for the competition. Rider training plans were developed based on team members' cycling training experience and online cycling resources, such as videos from Global Cycling Network (GCN).

1.5 Prior Work

This is the first time that UVA is taking part in the Human Powered Vehicle Challenge. All vehicle design and manufacturing was conducted during the 2019-2020 school year.

1.6 Organizational Timeline

A high-level overview of the schedule can be seen in Tables I-II.

Table I: Design Schedule for Fall Semester

Items	Week								
	Aug 27 - Oct 12	Oct 13-19	Oct 20-26	Oct 27- Nov 2	Nov 3-9	Nov 10-16	Nov 17-23	Nov 24-30	Dec 1-7
Preliminary Design Exercises & Team Formation									
Biomechanics Research									
Full CAD Design and Manufacturing Plan									
FEA+CFD Testing									
Generate Purchase List and BoM									

Table II: Manufacturing and Testing Schedule for Spring Semester

Items	Week										
	Jan 19-25	Jan 26 - Feb 1	Feb 2-8	Feb 9-15	Feb 16-22	Feb 23-29	Mar 1-7	Mar 8-14	Mar 15-21	Mar 22-28	Mar 29 - Apr 4
Frame Manufacturing											
Fairing Construction											
Drivetrain Installation											
Steering Assembly											
Safety Components Added											
Vehicle Testing & Design Iterations											
Design Report											

1.7 Product Design Specifications

ASME design specifications are displayed in Table III. The team added additional self-imposed specifications in order to make the vehicle more competitive and are shown in Table IV. The stronger specifications were determined from metrics from previous successful teams at HPVC, coupled with reasonable expectations for the team's first time competing.

Table III: 2020 ASME Design Specifications

Performance	<ul style="list-style-type: none"> • Brake from 25 km/hr in 6 m • Maintain a minimum turning radius of 8 m • Maintain stable travel from 5-8 km/hr for 30 m
Rollover Protection System (RPS)	<ul style="list-style-type: none"> • Protect driver in a continuous hoop • Provide abrasion resistance to protect the driver's arms and legs • No permanent deformation, fracture or delamination • Maximum elastic deformation of 5.1 cm from a top-load of 2670 N at an angle of 12° from vertical • Maximum elastic deformation of 3.8 cm from a side load of 1330 N inwards at a driver's shoulder height
Safety	<ul style="list-style-type: none"> • Wear bike helmet at all times when in vehicle • Wear closed-toe shoes • Each driver must have a minimum drive time of 30 min before the competition • No protrusions, sharp edges, open tube ends, and screws on the exterior or interior of the vehicle • Minimum field of view of 180° • Safety harness with lap and shoulder belt attached to the structural member • Braking system on the front-most wheel • Design and manufacture a steering mechanism with little to no play • Modifications between events cannot compromise the safety of the vehicle

Table IV: UVA 2020 Self-Imposed Additional Specifications

Performance	<ul style="list-style-type: none"> • Brake to a complete stop from 25 km/hr in 5 m (1 m less than ASME specification) • Maintain a minimum turning radius of 3.65 m (45% of ASME specification) • Obtain a maximum speed of 40 km/hr • Coefficient of drag between 0.2 and 0.3
Rollover Protection System (RPS)	<ul style="list-style-type: none"> • Maximum elastic deformation of 3.825 cm (75% of ASME specification) from a top-load of 2670 N at an angle of 12° from vertical • Maximum elastic deformation of 2.85 cm (75% of ASME specification) from a side load of 1330 N inwards at a driver's shoulder height • Place the overall center of mass in the front half of the wheelbase for lateral stability at high speeds (66% front/33% rear weight distribution)
Other	<ul style="list-style-type: none"> • Accommodate drivers from 5'4" to 6'3" • Maximum total weight of 27.5 kg • Achieve a frame safety factor of 2.0 compared to ASME specifications for top and side loading with respect to yielding • Riders complete a minimum of 2 endurance workouts per week in the fall, 2 strength/endurance workouts in the spring • Accommodate cargo of 5.5 kg with dimensions of 38 x 33 x 20 cm • Design and manufacture a vehicle using current funds of \$6500 or less

1.8 Concept Development and Design Selection

To determine final design selections, the team created design matrices. The matrices were broken down into two sections: one to determine the importance of the criteria, and the other to determine the effectiveness of the specific design. The weights were determined by a numeric scale ranging from one to three, with one being the least and three being the most

important. The design total scoring the highest product of the criteria importance and design effectiveness was chosen to be the best selection.

1.8.1 Frame and Fairing Design

The Frame and Fairing subteams worked in parallel to design an effective structure for the vehicle. The following section provides insight into the team's design decisions with respect to the overall vehicle geometry and selected materials.

The team initially decided on a recumbent design due to its advantages in speed and comfort for users, aligning with the team's objectives. The team looked into a bicycle or tricycle design (both tadpole and delta style) and ultimately decided that a tricycle design was best for stability and ease of use at low speeds. When deciding between a tadpole-style and delta-style, the team considered turning-radius and speed to determine whether tadpole or delta is more optimal. A tadpole design has a smaller turning radius and is less likely to turn-over, so the team decided on a tadpole configuration for the vehicle.

The team considered different materials for the frame: 4130 steel, aluminum, titanium, and carbon fiber. Each material was evaluated on its strength, fatigue, manufacturability, rusting, environmental impact, and cost. These criteria were selected to optimize safety (material strength) and durability (fatigue life and rust protection) while creating a low cost, easy to manufacture vehicle that is still environmentally friendly. Criteria weights were selected by importance to consumers as understood from the survey sent out. From the design matrix shown in Table V, 4130 steel and titanium were the highest rated. However, because 4130 steel is commonly used in recumbent trikes and easy to weld, it was chosen as the team's frame material.

Table V: Frame Design Decision Matrix

Criteria	Weight (1-3)	Titanium	4130 Steel	Aluminum	Carbon-Fiber
Strength	3	3	3	1	3
Fatigue Life	2	3	3	2	3
Manufacturability	3	2	3	1	2
Rust Protection	1	3	2	3	3
Environmental	2	3	2	1	2
Cost	3	2	3	3	1
Totals		36	39	24	31

The frame consists of tubing with outer diameters of 1.25 in., 1.00 in., and $\frac{7}{8}$ in. with a wall thickness of 0.065 in. The pipes were TIG welded together at the adjoining end of the pipes to complete a frame to protect the rider from collisions and abrasions (Fig. 1.3).

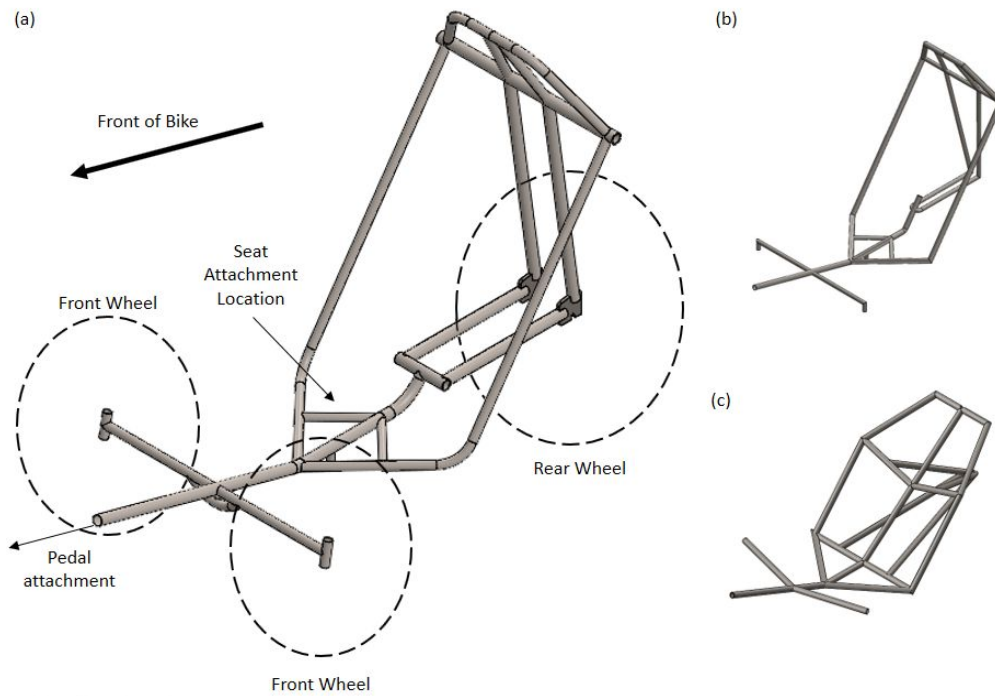


Fig. 1.3. Frame design iterations. The final frame design (a) uses bends in the pipe to reduce the number of welded connections, when compared to the previous version (b). An early iteration (c) uses much more material and features sharp corners in the design.

The team considered both a full and a partial fairing design. The final decision was made using a design matrix Table VI. The design criteria were selected to accommodate the vehicle's objectives of safety, speed, and practicality. Like the frame design, the criteria weights were selected to reflect the importance to consumers, as demonstrated in the survey results.

Table VI: Fairing Decision Matrix

Criteria	Fairing Type		
	Weight (1-3)	Partial	Full
Weight	3	3	1
Aerodynamics	3	1	3
Safety	3	1	3
Field of View	2	3	2
Manufacturability	2	2	2
Total		25	29

A full fairing outperforms a partial fairing in aerodynamics and safety, so the team chose to move forward with a full fairing and started exploring various iterations of the fairing. The team also had to choose between using thermoplastic foam and carbon fiber. To understand how difficult it would be to use foam, the team acquired free samples of thermoplastic foam from Worldwide Foam. Different density samples were molded using wooden male and female parts. The heat-treated foam samples can be seen in Fig. 1.4.

It is difficult to observe a difference from Fig. 1.4, but during the process, the fairing subteam felt a noticeable difference in the formability depending on density. Although the final product held the mold's shape, it was structurally weak. Despite the foam being significantly less dense than carbon fiber, there were concerns about how it would hold its form at high speeds.

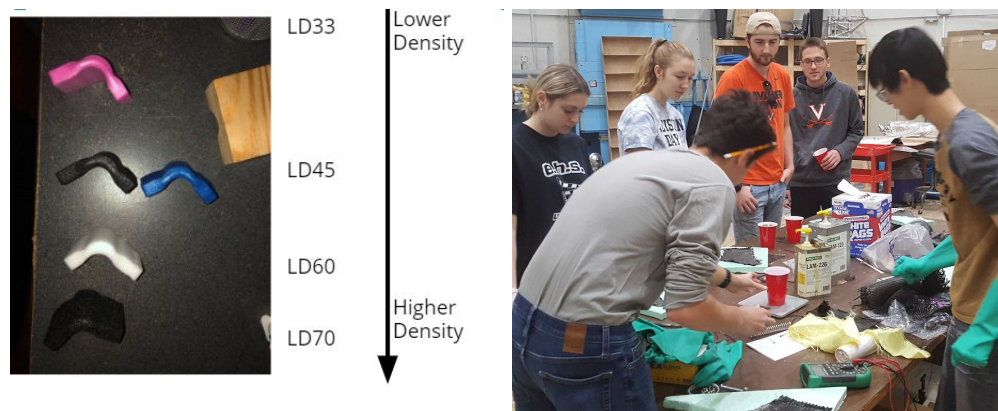


Fig. 1.4. Heat treated and molded LD (low-density) foam, number indicates density in kg/m^3 (left). Fairing team members practicing carbon fiber wet layup process (right).

The team also practiced carbon fiber fabrication. All of the composite manufacturing methods like preparing the mold, cutting carbon fiber, applying resin and hardener, and vacuum sealing were tested. The result was a very lightweight and strong carbon fiber piece. The carbon fiber test piece was significantly stronger and comparable weight to the foam. The team chose carbon fiber as the fairing material as they were more comfortable with the manufacturing process.

To select the final design, the Fairing subteam developed several iterations of the design. Initially, the team put a great focus on driver visibility and thought about window placement. The first few fairing designs have a sloping front that curves as close to the driver's head as possible. The goal of this was to be able to make the window as small as possible while not sacrificing aerodynamic advantages.

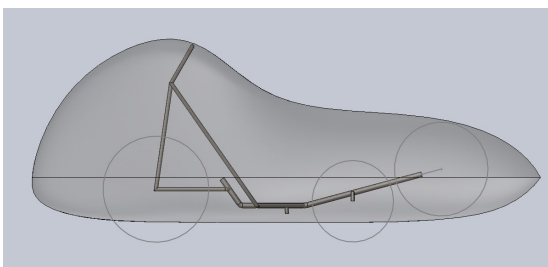


Fig. 1.5. Fairing design enclosing RPS and sloping front to help visibility

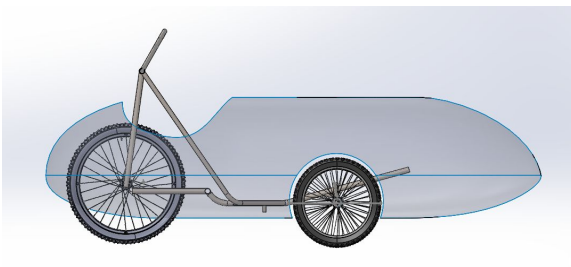


Fig. 1.6. Fairing design exposing RPS and driver's head

However, after further testing of the design, it was found that this curve adds a large amount of frontal area and also sacrifices aerodynamics as the slope of the window curve increases. The team decided to create a design where the driver's head and the top RPS are not completely enclosed.

As can be seen, the design in Fig. 1.6 significantly reduces the frontal area while also utilizing a much more aerodynamically favorable shape. Initial results support the exposed RPS design and the team moved forward with this design. In order to allow necessary wheel turning capability, cut-outs will be made around the front wheels (Fig. 1.7).

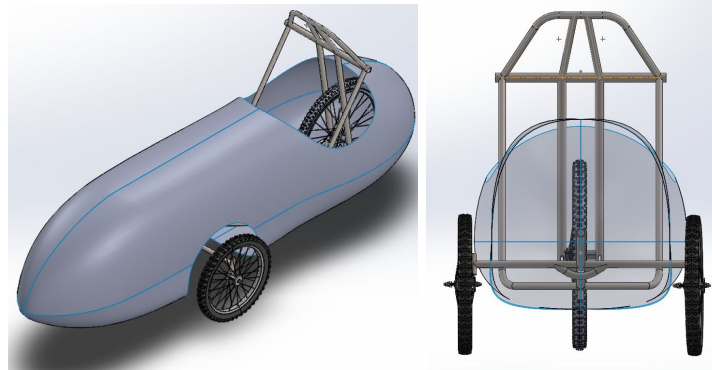


Fig. 1.7. Isometric (left) and front (right) views of final fairing design

To allow access for the rider to enter the vehicle, the top half of the fairing will be completely removable. This should allow for ease of entry and exit while also making the structure and drivetrain of the bike easily accessible for repairs. The lower half of the fairing is to be permanently attached to anchor points on the frame, while the top half will be secured to the bottom half through a series of latches.

1.8.2 Component Selection

The Drivetrain subteam researched archived HPVC design reports and consulted bikes@Vienna for component choices. Based on the advice of the recumbent bike shop owners, the team decided against using a front derailleur to minimize the possibility of the chain falling off the front chainring during use. At first, the team considered using a seat on sliding rails for adjustability. However, the safety and rigidity of such a design were a major concern. After consulting designs at bikes@Vienna, a chain gobbler with a telescoping boom was selected because it permits a fixed seat design while still allowing adjustments for different leg lengths.

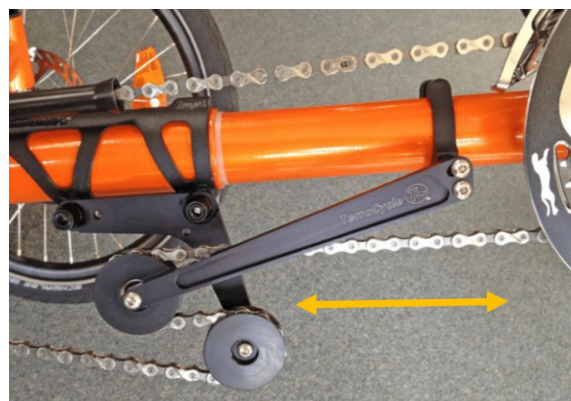


Fig. 1.8: Chain gobbler on a tadpole trike. Each idler wheel is fixed to their respective parts of the telescoping arm. As the arm changes in length, so does the distance between the idler wheels. As a result, the chain remains taut for any length of the arm (Catrike Boom Adjust Chain Tensioner, 2018).

A chain gobbler consists of a telescoping boom that uses two idler wheels to keep the chain taut while boom length changes. With one idler wheel fixed to the frame and the other fixed to the telescoping arm, the change in displacement of the idler wheels is proportional to the change in position of the front crankset, so the pedal distance can be moved without changing the chain length. The rest of the chain will be directed using power and return idler wheels to drive the rear wheel. The team designed circular clamps similar to stock chain gobbler clamps to hold each idler wheel in place along the tubes (Fig. 1.8). A 3 mm wide slot will be cut into the stationary outer tube to allow deflection from tightening the clamp.

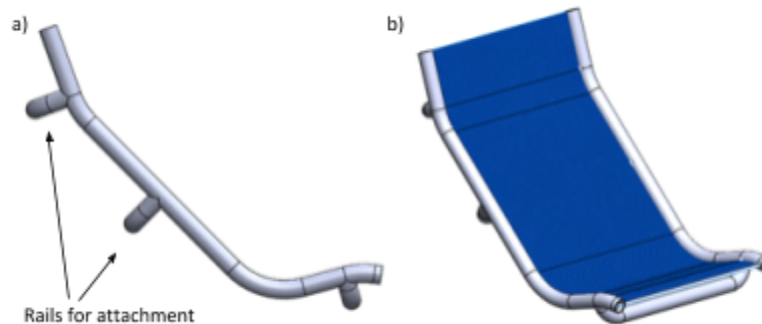


Fig. 1.9. Initial seat design. This would attach to the central pipe of the frame. View (a) shows a profile view of the seat with attachment rails; view (b) shows an isometric view of the seat.

After deciding on a fixed seat position design permitted by the addition of the chain gobbler, the team came up with several designs for the seat. The team first designed an independent mesh seat that could be welded to the frame's central pipe (Fig. 1.9). A metal frame would be made to hold the mesh in place. However, this design presented several concerns. With few attachment points, the seat is prone to mechanical failure and unsafe. A steel seat frame would be heavy and an aluminum seat frame would be difficult to weld to the steel vehicle frame.

To brainstorm alternate designs, the team consulted existing commercial recumbent bicycle designs. Commercial models such as the Catrike 700 feature a mesh seat integrated directly into the frame. This design reduces the weight of the seat frame and is much more stable and safe for riders. The drivetrain subteam collaborated with the frame subteam to pursue this idea.

However, there were more concerns with using mesh for the bottom of the seat. Mesh deflection from the riders' weight needed to be accounted for and the frame design did not allow for such space and put the rider sitting essentially on the frame's steel piping. The team decided to keep the seat back as mesh, but replace the bottom mesh with a solid padded piece. The final design uses a commercially available erg cushion, which is buckled onto a steel plate, as shown in Fig. 1.10.



Fig. 1.10. Seat integrated into the frame design.

Next, an 11-speed 11-46T rear cassette and compatible medium cage rear derailleur were selected to introduce a wide range of gear ratios limited by a single-speed front chainring. The team decided to order a single-speed, 38/28T front chainring to test and use separately in the speed and endurance events if needed. Details on gear ratio calculations considering the vehicle and competition specifications are in section 2.5.2. The team considered 11-speed bar end and trigger shifters but decided on using bar end shifters so that the steering handles could be comfortably positioned vertically with fewer bends to reduce friction while shifting.

Multiple braking systems were considered for cost, effectiveness, and ease of implementation. The team considered rim and disc brakes. Disc brakes consist of a metallic rotor at the center of the wheel and use calipers to clamp down on the rotor to braking, while rim brakes use a similar mechanism on the outer edges of the wheel. While rim brakes are cheaper, mud and water build-up render them inefficient and they perform poorly in high temperatures due to the friction and wear on the brake pads. Disc brakes were chosen because they do not require a direct connection to the frame, have a higher braking capacity, and are easily implemented.

Four types of steering placement were considered for the vehicle: over-seat, under-seat direct, under-seat indirect and tilt steering. Each steering placement was evaluated on integration into overall design, ease of use, maneuverability, and manufacturability in Table VII. These criteria were selected to create a feasible and functioning steering system. Criteria weights were selected to reflect team member's perceived priorities for the build.

Tilt steering has the best stability and navigation and is also better for endurance with bumpy road conditions but involves 3-dimensional steering kinematics which became inapplicable for the team. Over-seat steering is only applicable for delta trikes, and since the team decided to use a tadpole trike, the team's choices were limited to either direct or indirect steering placement. As shown in Table VII, the team chose indirect under-seat steering since its front two wheels turn at different radii, preventing vehicle skidding at high velocity and minimizing wheel vibrations transferred through the handlebars.

Table VII: Steering Design Decision Matrix

		Steering Placement			
	Weight (1-3)	Over-Seat	Under-seat (direct)	Under-seat (indirect)	Tilt Steering
Integration	2	1	3	3	1
Ease of Use	3	3	1	3	2
Maneuverability	3	2	3	2	3
Ease of Manufacture	2	3	3	3	1
Total		23	24	27	19

The steering system consists of two T-shaped plates, two tie-rods, a long rubber band that connects the end of T-shaped bars, a short connection bar, and several ball joint linkages. The short bar that connects the steering system to the frame will be manufactured from 6061 Aluminum plates using a waterjet cutter, and a T-shaped bar will be produced using a 4130 steel plate. The tie-rods are made of carbon fiber tubes with 0.5-inch inner diameter and 0.584-inch outer diameter, connecting the short bar to the long bar at the front with ball joints connections as shown in Fig. 1.11.

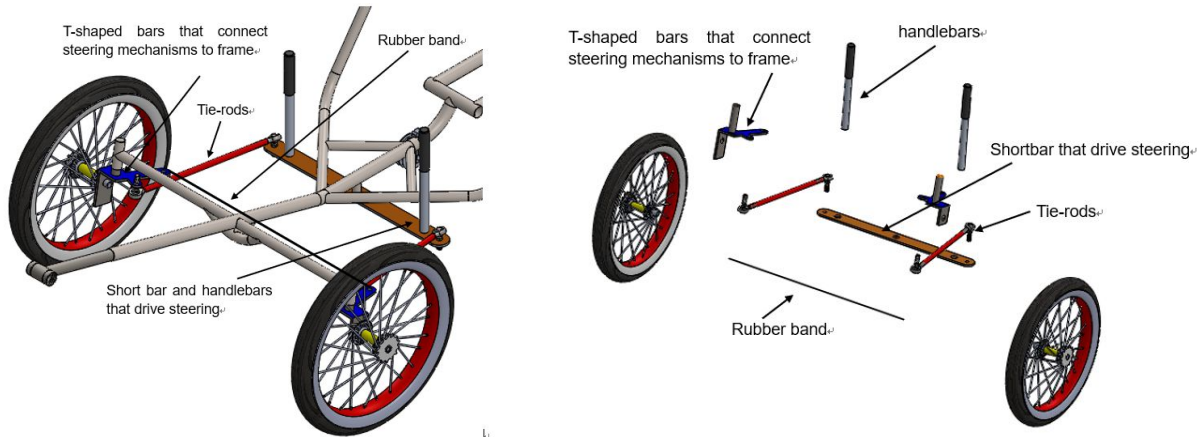


Fig. 1.11. Steering mechanisms collapsed (left) and exploded view (right)

For the steering mechanism, handlebars are connected to the short bar pivot which is attached to the frame on an axis under the seat. Tie-rods connect the short bar plate to the T-shaped bars which are used to turn the wheels. The steering subteam initially considered a traditional tie-rod linkage, but then realized T-shaped bars sit at a different height than the short bar. Therefore ball joints were used at the tie-rod connections, allowing the tie-rods to swivel up by 2.16° , as shown in Fig. 1.12. The tail of the T-shaped bars were initially connected by a solid aluminum linkage, but the team realized the distance between the T-shapes would vary while steering, and the aluminum linkage was replaced with a rubber band. A 10° positive caster angle was added to the wheels, adding a degree of steering self-centering to improve the vehicle's maneuverability and reduce its tendency to wander, as shown in Fig. 1.13.

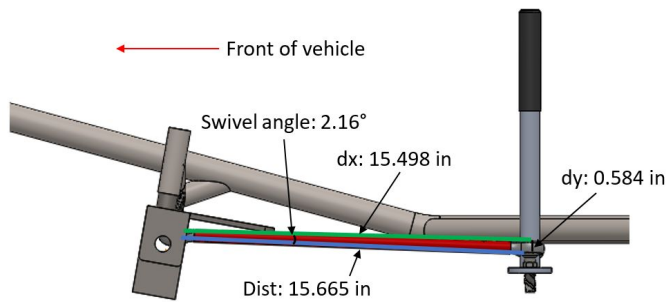


Fig. 1.12. Swivel angle and clearance of tie rods

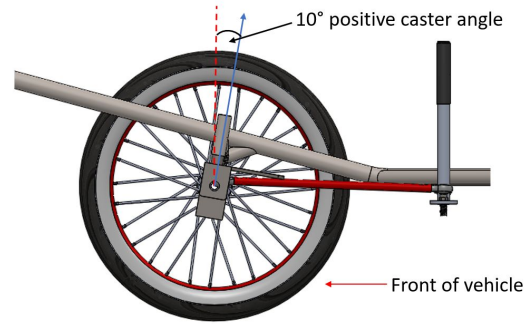


Fig. 1.13. Caster Angle Diagram

1.8.3 Safety and Electrical System

The team decided to implement headlights, brake lights, and sidelights onto the vehicle. The team decided to develop an electrical architecture around a 12 V rechargeable lithium-ion battery with 6000 mAh and an Arduino Uno R3 microcontroller. The electrical architecture was chosen to maximize efficiency and comfort, but most importantly, safety. The battery was chosen to satisfy the LEDs' voltage requirements and to power the lights for a minimum of two hours. As for the microcontroller, an Arduino was chosen due to its low price and ease of use.

A high level overview of the electrical system is shown in Fig. 1.14; a more in depth version can be seen in Appendix C. The system uses input buttons/switches connected to the Arduino to detect if the driver has signaled to brake or turn.

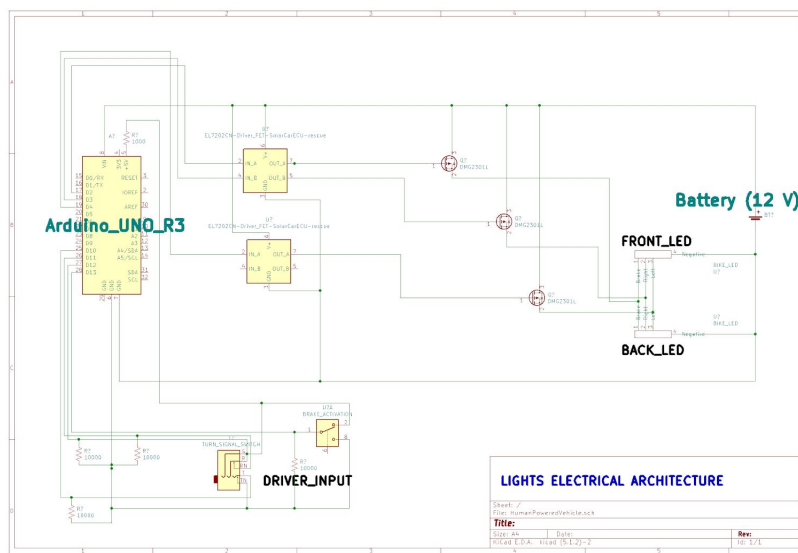


Fig. 1.14. Electrical architecture to control and power vehicle lights

1.8.4 Environmental Design Considerations

To support the team's goals of creating a sustainable, practical vehicle, archived HPVC design reports were consulted to understand how teams reduced their carbon footprint. The University of Pittsburgh's 2017 report stated that material refining, steel production, and electricity usage were all important considerations for carbon emissions (Stucky, 2017). Therefore, these aspects were considered to also be the most important for the construction of

the vehicle. To understand the carbon footprint of each aspect, carbon emissions for various processes were researched to understand how to approximate accurate emissions. A study from Carnegie Mellon University approximated the theoretical minimum energy emissions from the material refining of iron ore and oxygen furnace steelmaking to be 8620 MJ/tonne of ore and 7900 MJ/tonne of steel, respectively (Fruehan, 2000). Studies from the U.S. Energy Information Administration stated that on average, 93.3 kg of CO₂/MBtu is created for refined coal electricity, (U.S.EIG, 2016).

The team initially considered earning a carbon footprint certificate through the Carbon Fund; however, due to cost, the team decided not to certify the vehicle, but to calculate the carbon footprint and compare it to the footprint of a mid-sized internal combustion engine vehicle.

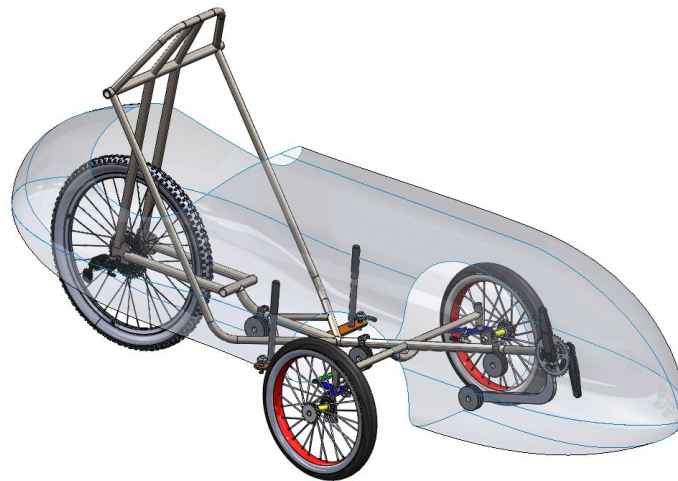


Fig. 1.15. Full assembly of final vehicle design

1.9 Design Description

In summary, the Smithinator is a tadpole type recumbent tricycle, as shown in Fig. 1.15, powered by a rear 700c wheel, an 11-46T rear cassette, and a 38/28T front chainring. The positioning of the pedals is made adjustable through the use of a chain gobbler to accommodate riders of different heights. An indirect under-seat Ackermann steering system is implemented to allow the front two wheels to have different radii and avoid skidding while turning. The vehicle has a full carbon-fiber fairing which allows for considerable weight reduction, improving speed performance and reducing drag force that would otherwise contribute to quicker fatigue of the rider. Additionally, the fairing design will improve safety, preventing smaller debris and weather elements from reaching the rider. The recumbent tadpole design is more stable at high speeds than a delta tricycle and has a lower center of gravity than an upright bike.

2. Analysis

2.1 RPS Analyses

2.1.1 Objectives, Methods, and Assumptions

Finite Element Analysis (FEA) was conducted using SolidWorks on the frame to determine if the RPS designed met ASME's specifications and the team's own specifications for top and side loading. For RPS analyses, the simulation was constrained at the safety harness mountings in order to analyze the RPS safety within the driver's frame of reference. The RPS components

were assumed to be made of linear-elastic, homogenous, isotropic solid steel modeled as beams in the analysis. Furthermore, the deflections are assumed to be small.

2.1.2 Top Load Analysis

The top-loading analysis shows the case of the vehicle flipping and landing upside down. The load from this scenario is simulated with a force of 2670 N at a 12° angle with the vertical to the top of the RPS at its midpoint to simulate the loading required by ASME specifications. The constraints for the frame model during FEA were placed at the joints associated with the mounting of the harness as seen in Fig. 2.1. The results from the top-loading can be seen in Fig. 2.1. The analysis showed a max deflection of 1.25 mm, located on the top of the RPS and the back of the rear fork, which is well within the max allowable deflection specified by ASME of 5.1 cm. In addition, the structure of the frame dissipated the load as it traveled to the bottom of the frame. The factor of safety (FOS) for yielding for the top-loading was 2.7 for yielding, which is above the team's imposed specification of an FOS of 2.0.

2.1.3 Side Load Analysis

In the case of the side-loading, the analysis shows the case of the vehicle turning over and landing on its side. As with the top-loading, constraints were placed at the joints associated with the mounting of the harness as seen in Fig. 2.2. To simulate the vehicle on its side, a force of 1330 N at around shoulder height for a rider on the side of the RPS that would make contact with the ground to simulate the loading required by ASME specifications. The side-loading displayed a max deflection of 3.70 mm, which is located on the side of the RPS and the front of the boom (Fig 2.2), and is also within the specification of 2.85 cm. The FOS for the side loading was 1.625, though below the team's imposed specification of a FOS of 2.0, it still meets ASME's specifications.

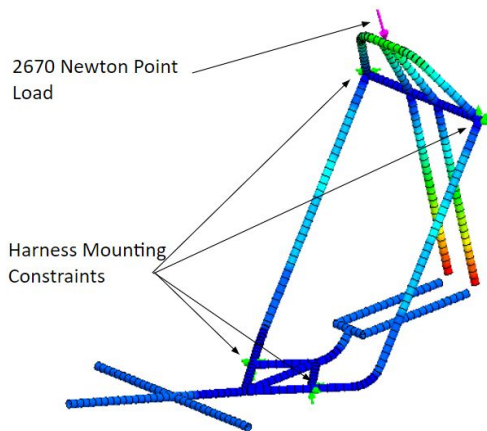


Fig. 2.1. Top loading displacement with ASME specifications

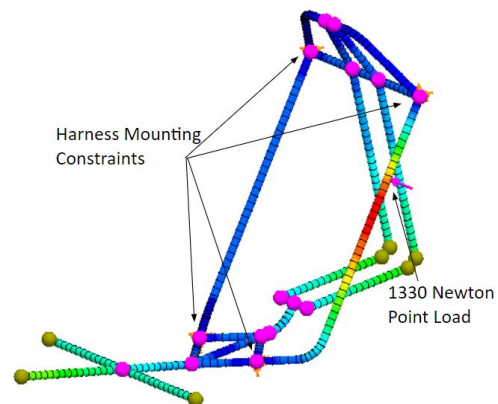


Fig. 2.2. Side loading displacement with ASME specifications

2.2 Structural Analyses

2.2.1 Rider Weight and Pedal Box Analysis

Additional FEA load scenarios have also been tested. Load scenarios for the simulation of pedaling and the rider's body weight were conducted to confirm that the integrity of the frame is maintained once a rider is placed inside. FEA on the seat was conducted to ensure that a rider can sit on it without much deformation as seen in Fig. 2.4. The team simulated a 180 lb person

sitting within the frame by applying a downward force of 180 lb at the point where the seat is at the base of the frame. Fixtures were placed at the locations where the wheel attachments are. The minimum FOS for the case of simulating the weight of a 180 lb person was 3.0 and the max displacement was 8.8 mm ,with the most significant amount of stress at the point of applied loading and where the central boom attaches to the steering boom (Fig 2.4).

To simulate a rider pedaling the team place a torque of 300 N · m at the location of the pedals at the end of the boom as shown in Fig. 2.3. Rider biometric data demonstrated a max torque value of 256.1 N · m. As the riders are conducting training two times a week the torque in the simulation was increased to 300 N · m to account for riders getting stronger. Results from the study show a minimum FOS of 1.59 and a max displacement of 2.42 mm, with the largest amount of stress located at the end of the boom where the pedals are located (Fig 2.3).

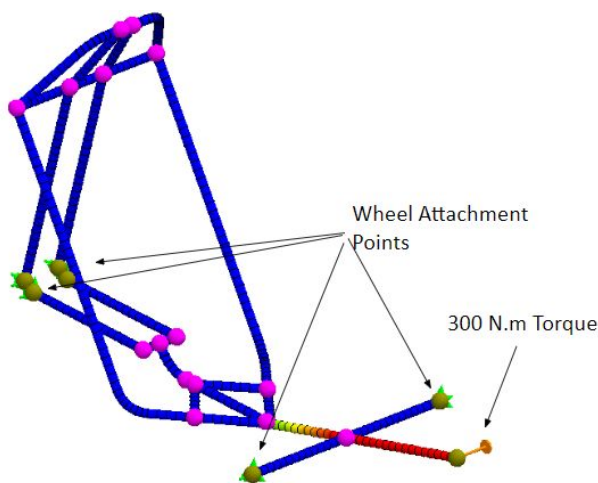


Fig. 2.3. Pedal Box FOS with ASME specifications

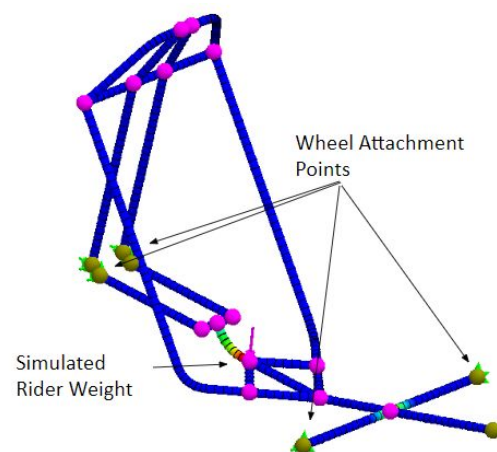


Fig. 2.4. Rider weight simulation FOS using point load

2.2.2 Seat Analysis

The amount of deflection at the bottom of the seat was measured to determine the feasibility of the design. A distributed load of 800 N was applied to the foam cushion to represent a 180 lb person, and the support fixtures were distributed across the bottom of the steel plate (Fig. 2.5). A maximum deflection of 1.29 mm into the foam is well under acceptable deflection measurements of 8 cm, as determined by Severy et al. (1976). This study is limited by the uncertainty of exact foam density and cushion properties but will be used as a general estimate for determining steel plate thickness.

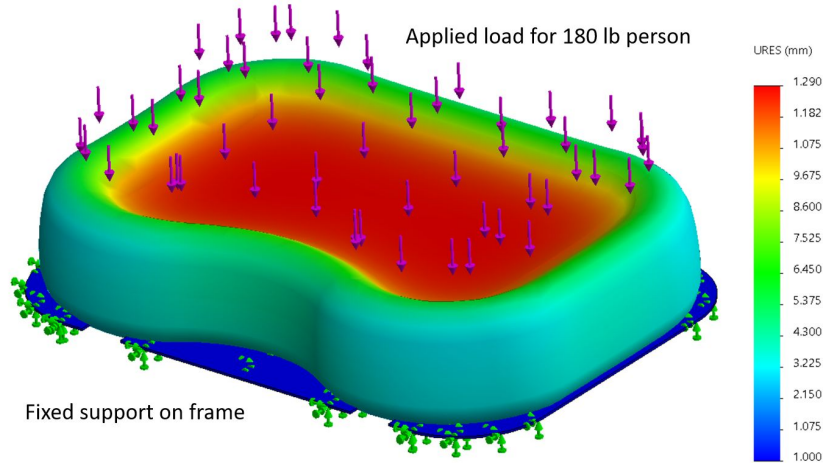


Fig. 2.5. Analysis of bottom seat deflection when integrated into frame

2.3 Aerodynamic Analyses

2.3.1 Objectives, Methods, and Assumptions

An aerodynamic analysis was conducted to optimize fairing design to minimize the coefficient of drag and weight. Using Autodesk CFD, the team placed the fairing CAD model into a control volume box and then assigned the boundary conditions and material settings. The fairing material was set as solid ABS (polycarbonate) and the enclosure material was selected to be air. The enclosure wall facing the front of the fairing was given a velocity boundary condition set at 20 mph. The wall at the back of the fairing was given a static pressure condition of 0 psi. The other four walls were given slip/symmetry boundary conditions. Fig. 2.6 depicts the boundary condition settings utilized.

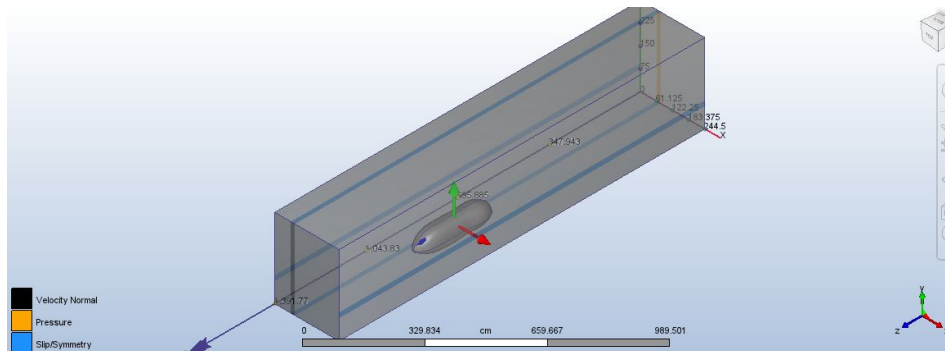


Fig. 2.6. Boundary conditions of CFD analysis

After running CFD on a design, the team analyzed the points of pressure loss and turbulence generation. This spatial information is used to modify the geometry at the specific points to reduce aerodynamic loss. The drag coefficient was calculated by taking the drag force from the CFD simulation, finding the section area in SolidWorks, and using the following equation.

$$C_D = \frac{2F_D}{A\rho V^2} \quad [\text{Eq. 1}]$$

2.3.2 Results and Conclusions

The CFD results support an open cockpit. The design that fully enclosed the RPS was found to have a drag coefficient of 0.35 and a drag force of 11.59 N. The design that leaves the driver's head exposed had a drag coefficient of 0.32 and a drag force of 7.36 N (Fig. 2.7).

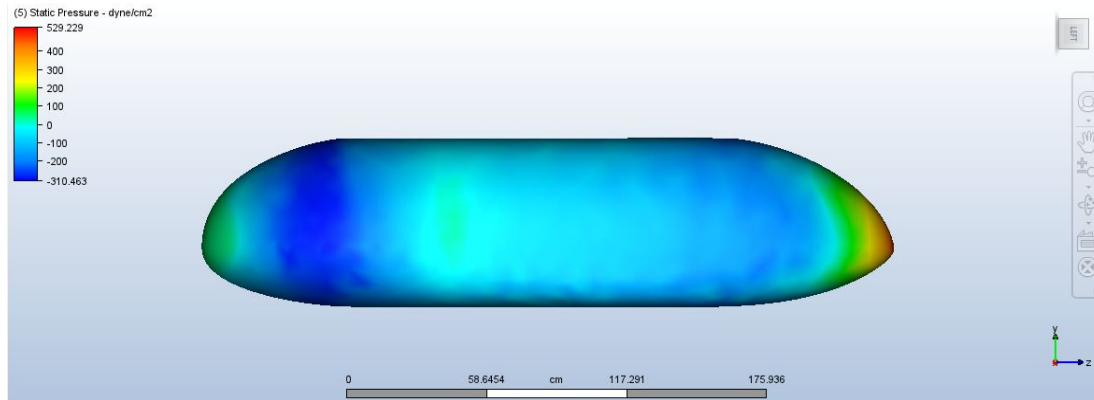


Fig. 2.7. CFD results of selected design from the side view (front of vehicle on right). Red indicates high pressure.

Throughout the testing process, factors that seemed to be important in effective designs were identified. Minimizing the cross-sectional area was very critical and a large reason for choosing the design. It is important to keep the shape of the fairing as uniform and smooth as possible. This was difficult when trying to leave enough room for the driver's body and the turning of the wheels, but was a key focus when trying to preserve aerodynamics.

These CFD results were used to minimize areas of high pressure. The team's goal was to reduce the drag coefficient to under 0.3, which seemed to be the range where many competitive vehicles fall. The target drag coefficient was not able to be achieved. Design adjustments required more clearance for parts of the bike than originally expected, increasing the cross-sectional area thus increasing drag. However, the exposed head design was still able to outperform the fully enclosed design with a lower drag coefficient and drag force.

2.4 Cost Analyses

The vehicle was constructed from a total budget of \$6,500. The funding was provided by the University of Virginia's Mechanical Engineering Department, the School of Engineering and Applied Sciences' Experiential Learning Fund, and UVA Parents Fund totalling funds of \$2,000, \$2,500 and \$2,000, respectively. The construction cost for the vehicle totals to \$4,065.91 as shown in Table VIII, which is 62.6% of the total budget. Major cost components of the project include steel for the frame, carbon fiber for the fairing, clipless shoes for each driver, and the tires and wheels. The machinery needed to manufacture and assemble the vehicle was available and provided by the University of Virginia. No third-party labor costs were required due to the purchase of pre-manufactured parts and self-manufacturing by team members. The remainder of the total budget was used for registration and travel expenses. An in-depth breakdown of costs by subteam can be seen in Appendix D.

Table VIII: Cost Breakdown by Subteam

Cost Type	Subteam	Cost
Construction	Frame	\$759.70
	Drivetrain	\$1,281.91
	Fairing	\$1,277.70
	Steering	\$420.68
	Innovation	\$184.54
	Safety	\$87.88
	Tools	\$53.50
	Total	\$4,065.91

2.5 Other Analyses

2.5.1 Ackermann and Turning Radius Analysis

The steering system features Ackermann geometry. This geometry allows the turning angles of both front wheels to share a common center point which lies on the same axis with the center of the rear wheel (Fig. 2.8). The Ackermann geometry allows the inside front wheel to turn with a slightly greater angle than the outer to prevent scrubbing while turning. Initial Ackermann and turning radius calculation used Peter Eland's spreadsheets for Ackermann steering linkage design.

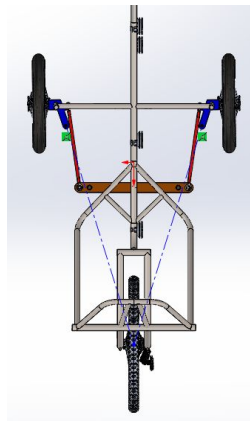


Fig. 2.8. Ackermann top view

The team set a self-imposed goal of a 12 ft (3.65 m) minimum turning radius of. The Ackermann design allowed the center of the vehicle to remain on a constant radius around the center of rotation. However, the front wheels in this system would rotate at different rates, meaning the wheels would have different turning radii and angles compared to the frame. Thus, the outer wheel turning radius should be used for the "true" turning radius. Appendix B shows the equation derivation for turning radius. As there is only one back wheel, c was set to be 0. This was tested with a maximum ψ angle of 25° , 0.8 m for a , and 1.197 for B . Thus, R was only 2.87 m, well under the goal of 3.65m.

The efficiency of our Ackermann steering was also tested. Under an ideal design, Ackermann wheels should turn at a certain rate in relation to one another, making sure that they create two circles about the center of the turning radius. As the turning radius decreases, the difference in angles between the two wheels becomes more noticeable. Error in the design was consistently low, ranging from 0.83% to 4.93%, shown in Table IX.

Table IX: Ackermann Steering Geometry Analysis

Turning Radius (ft)	Ideal Ackermann		Experimental Ackermann	
	Left wheel angle (°)	Right wheel angle (°)	Right wheel angle (°)	Error
12	16.66	20.87	19.84	4.93%
25	8.65	9.69	9.39	3.13%
50	4.47	4.74	4.66	1.64%
75	3.01	3.13	3.10	1.10%
100	2.27	2.34	2.32	0.83%

2.5.2 Drivetrain Gearing Analysis

In order to find the optimal chainring size based on resistive forces of air resistance, rolling resistance, gravity, and drivetrain efficiency, the team conducted a rough gearing analysis. A free-body analysis of forces was used to calculate power needed to climb a worst-case 5% grade incline. The formulas below were derived at the minimum velocity possible while pedaling at 60 rpm:

$$P_{needed} = (F_{air\ res} + F_{roll\ res} + F_{hill\ grav} + F_{efficiency}) * v_{min}^{gear\ ratio} \quad [Eq. 2]$$

$$F_{air\ res} = \frac{1}{2} \rho A C_d v^2 \quad [Eq. 3]$$

$$F_{roll\ res} = \mu N = \mu W \cos(\tan^{-1} G) \quad [Eq. 4]$$

$$F_{hill\ grav} = W \sin(\tan^{-1} G) \quad [Eq. 5]$$

$$F_{efficiency} = 0.95 * F_{applied} \quad [Eq. 6]$$

where $v_{min}^{gear\ ratio}$ is the gear ratio from the Sheldon Brown Gear Ratio Calculator, G is the grade of hill the (%), C_d is the Coefficient of drag, ρ is the air density, μ is the coefficient of friction, A is the area, P_{needed} is the power needed to climb the hill, and W is the sum of the weights of the rider, cargo, and trike. $F_{air\ res}$, $F_{roll\ res}$, $F_{hill\ grav}$, $F_{efficiency}$ are the forces adding resistance against the motion of the vehicle.

The power the rider must exert to climb the hill was calculated and the outputs can be seen in Table X. The calculations assume a bike, rider, and cargo combined weight of 114 kg, a drag coefficient of 0.32, and bike frontal area of 0.465 m². Based on these formulas, a 38T front chainring is recommended in conjunction with the 11-46T rear cassette to maintain an optimal balance of max speed and power required (Table X).

Table X: Power Output and Speeds for 42T-34T Front Chainrings

	Front Chainring Size				
	42 Tooth	40 Tooth	38 Tooth	36 Tooth	34 Tooth
Minimum speed @ 60 rpm (uphill)	6.76 km/hr (4.2 mph)	6.44 km/hr (4.0 mph)	6.12 km/hr (3.8 mph)	5.79 km/hr (3.6 mph)	5.47 km/hr (3.4 mph)
Power needed to climb uphill @ 60 rpm	117.73 W	112.07 W	106.41 W	100.77 W	95.13 W
Max Speed @ 120 rpm (flat)	56.97 km/hr (35.4 mph)	54.39 km/hr (33.8 mph)	51.66 km/hr (32.1 mph)	48.92 km/hr (30.4 mph)	46.19 km/hr (28.7 mph)

Further analysis was done to better understand the role of each input variable on the power output based on drivetrain components and vehicle characteristics. Fig. 2.9 provides justification for the addition of the fairing in the design; even with the added weight of the fairing, the lower coefficient of drag reduces the power output needed by the rider to climb the hill. While the fairing does add more weight to the vehicle, the resulting decrease in drag makes it worth the estimated 5 kg weight increase. Keeping the fairing would require less power output than removing the fairing during the endurance event.

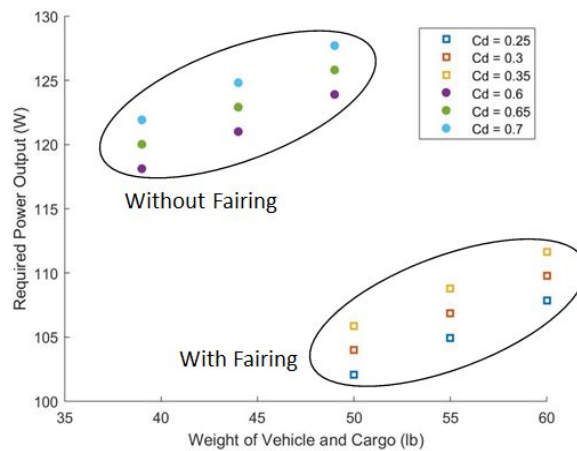


Fig. 2.9. Power output based on drag coefficient and weight

2.5.3 Center of Mass Analysis

A center of mass test was performed to ensure that the center of mass lies within the front third of the wheelbase as specified in the *Golden Rules of Trike Design* (Fenner, 2010). The center of the mass of the vehicle with the frame, fairing, 240 lb rider, and steering system is 15.8 inches (40.13 cm) behind the front axles according to the team's CAD assembly file. The center of mass, according to the CAD file, satisfies the ratio (wheelbase of 122 cm, or 48 in) (Fenner, 2010). The actual center of mass will be recalculated after the vehicle is manufactured, so a heavier than expected conservative rider weight was used in this calculation. The team expects that the final center of mass will shift forward, but still lie within the front third of the vehicle per a *Golden Rules of Trike Design* recommendation for lateral stability.

2.5.4 Product Lifecycle / CO₂ Analysis

As shown in Table XI, the tonnage of CO₂ will be totaled from three sections: material refining, steel production, and electricity usage. To calculate the emissions from material refining and steel production, as shown in Table XII, the weight of the iron ore and steel was approximated

and measured from the design drawings and manufacturing. To calculate the tonnage of CO₂ from electricity usage, as shown in Table XIII, the rated wattage from the equipment used was recorded from the equipment specifications. The time of use of the equipment was measured to calculate the energy usage in kilowatt-hours. To calculate the tonnage of CO₂ emitted, each section will be totaled to megajoules and then be converted to tonnes of CO₂ by the conversion factor of 8.84E-5 tonne of CO₂/MJ provided by the U.S Energy Information Administration (U.S.EIG, 2016).

Table XI: Total Life Cycle CO₂ Emissions

Total Carbon Dioxide Emissions		
Process	Type	CO ₂ (tonne)
Material Refining	Theoretical Minimum Energy	0.0105
Steel Production	Basic Oxygen Furnace	0.0096
Electricity	Refined Coal	8.40E-04
Total		0.0209

Table XII: Emissions Conversions from Material Processes

Material Processes					
Process	Material (tonne)	MJ/tonne of material	Energy (MJ)	tonne of CO ₂ / MJ	CO ₂ (tonne)
Material Refining	0.0138	8620	118.96	8.84E-05	0.0105
Steel Production	0.0138	7900	109.02	8.84E-05	0.0096

**Weight of steel includes weight of steel used on the frame and steel used to practice welds*

Table XIII: Emissions Conversions from Electricity Usage

Electricity					
Equipment Type	Equipment Wattage	Usage Time (hours)	Energy (MJ)	tonne of CO ₂ / MJ	CO ₂ (tonne)
Welder	66	40	9.5	8.84E-05	8.40E-04

To date, approximately 0.0209 tonnes of CO₂ was emitted from the manufacturing of the vehicle. Based on the average 5.6 tonnes from the production of a mid-sized internal combustion engine vehicle, the human-powered vehicle only emitted 0.37% of the CO₂ emissions compared to the average vehicle (LowCVP).

3. Testing

RPS Testing and Performance Testing have not been completed yet as the vehicle is still in the manufacturing stages. Plans for the tests are outlined in sections 3.1 and 3.3.

3.1 RPS Testing

RPS testing will verify if the manufactured frame meets ASME's and self-imposed specifications. After completion of the frame, the team will place weights on the frame to simulate different loading scenarios. For the top loading, the team will fix the base so it does not move while the weight is being placed on the top RPS. Weights will be placed incrementally on to the top RPS until the specified 2670 N is reached. The deflection will be measured with a dial gauge placed under the point at which the load is being applied. It is possible that with testing equipment the

team will not be able to simulate the load at the specified 12° from the vertical. Also, if possible the team will try to access a hydraulic press to simulate the load of 2670 N.

To test the side load, the frame will be fixed on one of its sides so that it does not move as the load is being applied. Loading will continue to be applied to the side RPS at around shoulder height until the ASME specification of 1330 N is reached. Again, the deflection will be measured with a dial gauge placed under the point at which the load is applied. As with the top loading the team will try to access a hydraulic press to conduct the test.

3.2 Developmental Testing

3.2.1 Biomechanics Testing

Biomechanics testing was done to determine optimal seat angle and position to maximize rider efficiency. Using a Biodex machine, the team recorded the torque outputs for each of the riders at various seat angles and seat distances from the pedals. The seat position range was determined by measuring riders' leg lengths, measured from the trochanter vertically to the floor in a standing position (TF distance), analogous to each riders' full leg extension on the bike (Fig. 3.1). The crank position was set at a constant 90° from the horizontal throughout all testing (Fig. 3.2). Riders sat on the Biodex and pushed as hard as possible against the crank for two seconds. Each rider performed three trials at 40°, 55°, and 70° seat angles (measured from the horizontal) at 100%, 104%, and 108% of their respective TF distance away from the crank, as recommended by literature studies (Shennum, 1976; Too, 1993). Trials were randomized to reduce the influence of rider fatigue on the data. A trial matrix can be seen in Table XIV.

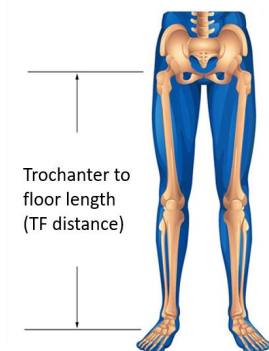


Fig. 3.1. Trochanter to floor distance

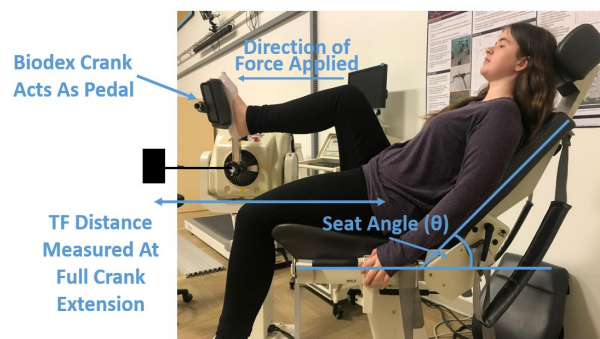


Fig. 3.2. Biodex setup (40° angle at 100% TF distance shown)

Table XIV: Biodex Testing Matrix

	Trochanter to Floor (TF) Distance		
	Seat Position = 100%	Seat Position = 104%	Seat Position = 108%
Angle = 70 deg	3 trials	3 trials	3 trials
Angle = 55 deg	3 trials	3 trials	3 trials
Angle = 40 deg	3 trials	3 trials	3 trials

The testing procedure initially included a 112% TF distance. However, upon running trials, the 112% seat position was deemed uncomfortable by riders, and the corresponding data showed significantly lower torque outputs resulting in subsequent removal from the procedure.

The maximum torque was calculated at each seat position for each angle (Fig. 3.3). Scatter plots of results can be found in Appendix A. After conducting an ANOVA test, the team concluded that the seat angle did produce significant results ($p=0.0365$). A post-hoc Tukey test revealed that there was a significant difference between the 40° and 70° angles, but there was no significance between 55° and 70°. To determine the final frame seat angle, the team considered aerodynamic advantages of the positions. Since a higher seat angle was speculated to have adverse effects, a 55° angle was chosen for the seat angle. Because the team is unable to conclude a significant difference across the seat position results ($p=0.406$), the team will use individual results to position the telescoping boom differently for each rider.

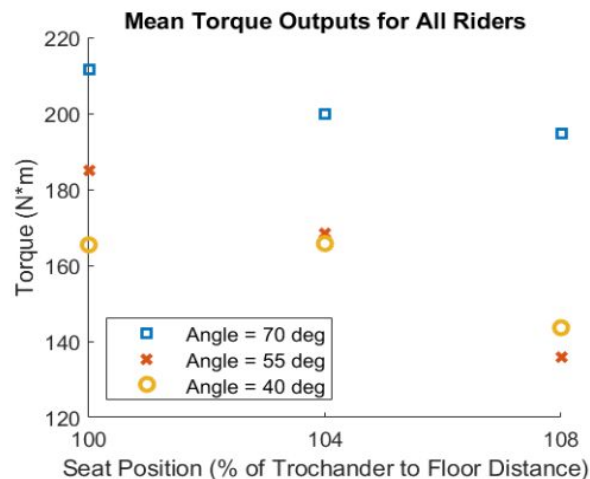


Fig. 3.3. Biodex Testing Mean Torque Output Across All Riders

3.2.2 Seat Development Testing

The team plans to perform testing on the material properties of several samples of mesh to identify the best mesh for the vehicle for comfort and durability. In particular, the team is looking at the strength of the mesh to ensure that it can withstand the applied load of the rider's back when pushing back during rides. Deflection of the mesh will determine how tightly to strap the mesh to the frame and how often it needs to be retightened. Riders will test seat cushions strap tightness over time and for any cushion movement while riding. Comfort will be judged qualitatively by riders during general performance testing and appropriate adjustments will be made. Results for this test will be presented at the competition.

3.2.5 Weld Development Testing

Developmental testing on the team's welds have yet to be performed. The team plans to perform a tensile test to test the strength of the welds of the 4130 steel pipes used for the frame to determine at what force they fail. A T joint will be used for this test. As the team is using pipes of different diameters at the location of many joints, the test specimen will consist of a 1" OD pipe welded to a 1.25" OD pipe.

3.3 Performance Testing

After the vehicle is manufactured, riders will verify the ASME required 8 m minimum turning radius and the team's self-imposed specification of 3.65 m on flat pavement. Speed and stability testing will be completed to verify the calculated top speed of 51.66 km/hr and ability

to maintain a straight line for 30 m at this speed. The team expects the vehicle to be stable at high speeds and will recalculate the center of mass location as final subsystem weights and configurations are determined. The team will test whether the vehicle is able to stop from a speed of 25 km/hr in 5 meters. As mentioned before results will be presented at the competition.

4. Safety

The RPS is necessary in order to keep the rider from impact with the ground in case of a rollover. As the frame subteam designed the RPS, careful attention was given to making sure that the rider did not come into contact with the ground if inverted. Also, the design of the frame was heavily dictated by what would provide the least amount of deformation as a result of ASME specifications for top and side loading. FEA was used to simulate the loads applied to the top and side of the vehicle (2670 and 1330 N respectively). The study showed a maximum deflection of 3.70 mm as a result of sideloading, and 1.25 mm as a result of top-loading, which is well under the ASME specifications for each load.

In order to provide a safe method of preventing upward and forward motion of the torso, a 4 point harness will be connected to the roll bar of the vehicle. It is important for the harness to be tight, adjustable, ergonomic, and easy to strap on. To optimize these functions, the Tanaka Phantom Series Buckle 4 Point Safety Set was selected. It provides durable shoulder pads to ensure comfort and security, has an easy release 1-second buckle system, and is relatively lightweight compared to other commercial options.

The steering and braking system will be tested once the vehicle is fully assembled. T-shaped plates play a crucial role in the steering system since they need to withstand torsion and bending forces, and they are also responsible for connecting wheels and frame to the steering system. The aluminum T-shaped plates were replaced with 4130 steel and further safety analysis will be conducted to ensure the integrity of the steering system and make sure the rider will not overturn the steering at sharp corners.

There are additional hazards that need to be accounted for. During the manufacturing of the frame and assembly of the vehicle, the team will be careful to avoid any sharp edges, protrusions, or pinch points. The chain may derail, so the team must make sure that a loose chain cannot hurt a rider or damage the vehicle. Carbon fiber is brittle, so precautions must be made to prevent the fairing from shattering.

ASME requires that riders have at least 180° of visibility. The open cockpit design satisfies this requirement. To allow for a greater range of visibility for the drivers, two side mirrors and a rearview mirror will be attached to the fairing to create a wider field view of the rear of the vehicle while reducing the risk of collisions. LEDs will be attached as a form of headlight and taillights, which will alert drivers in which direction the vehicle is turning, along with improving visibility at nighttime. A horn will also allow riders to quickly alert others of their presence.

Before the competition, all riders will be sure to submit ride logs that verify that they have adequate driving experience in the vehicle. They will wear enclosed shoes and appropriate

clothing, along with properly fitted helmets that meet the CPSC safety standard for bicycle helmets.

5. Conclusion

Table XV: Comparison of self-imposed specifications and analytical results

Design Specification	Targeted Result	Expected Result
RPS Top Loading (2670 N) FOS	> 2.0	2.70
RPS Top Loading (1330 N) Deflection	< 3.825 cm	0.125 cm
RPS Side Loading (1330 N) FOS	> 2.0	1.625
RPS Side Loading (1330 N) Deflection	< 2.85 cm	0.037 cm
Coefficient of Drag	$0.2 < C_d < 0.3$	0.32
Turning Radius	< 3.65 m	2.87 m

5.1 Comparison

As shown in Table XV, the team is predicted to exceed specifications in the factor of safety for the top loading, both deflections for top and side loading, and the turning radius. Though the results for the side loading factor of safety is less than the team's self-imposed specification, it is still well above a FOS of 1.0. While the coefficient of drag is also above the targeted goal, it is only slightly greater so the team is satisfied with this result. Actual performance results will be determined after the vehicle has been assembled.

5.2 Evaluation

The success of the vehicle was based on how well it met both ASME and the team's self-imposed design specifications. Since the assembly of the vehicle has not been completed at the time of the submission of the design report for the competition, not all the goals set out by the team can be fully evaluated. Table XV demonstrates that the team has achieved a favorable top loading deflection and turning radius. The side loading deflection satisfies ASME's requirements, but it does not meet the team's goal of a factor of safety of 2.0. The expected coefficient of drag of the vehicle is slightly higher than the imposed range, but still allows the team to be competitive. Other performance specifications, such as turn radius and acceleration, will be evaluated after the completion of the assembly and presented during the Design Presentation at the competition.

5.3 Recommendations

Though the team is still in the process of assembling the vehicle, there are some recommendations for the future. The design of the frame proved to be a challenge as issues with the initial design emerged near the start of manufacturing, causing our timeline to shift back. Some suggestions would be to consult the UVA machine shop resources at the start of the design process and more frequently to better understand the manufacturing capabilities possible for a chosen concept. The team should make a plan for all of the welding connections. Future UVA teams should finalize designs, fittings between subteam parts, testing plans (RPS, performance, safety, etc.) and have all components shipped by the end of December for a smooth manufacturing process, all while communicating between subteams to crosscheck progress.

6. References

- Amazon.com : Shimano PD-M520 SPD Clipless MTB Bike Pedals - Black : Sports & Outdoors. (2019). Retrieved from https://www.amazon.com/Shimano-PD-M520-Clipless-Bike-Pedals/dp/B07R16ZW25/ref=asc_df_B07R16ZW25/?tag=hyprod-20&linkCode=df0&hvadid=343991624868&hvpos=1o1&hvnetw=g&hvrnd=3884760576903533669&hvpone=&hvptwo=&hvqmt=&hvdev=c&hvdvcmdl=&hvlocint=&hvlocphy=9008337&hvtargid=pla-762089358398&psc=1&tag=&ref=&adgrpid=69358347255&hvpone=&hvptwo=&hvadid=343991624868&hvpos=1o1&hvnetw=g&hvrnd=3884760576903533669&hvqmt=&hvdev=c&hvdvcmdl=&hvlocint=&hvlocphy=9008337&hvtargid=pla-762089358398
- Amazon.com : SHIMANO SH51 SPD Cleat Set : Replacement Cycling Cleats : Sports & Outdoors. (2019). Retrieved from <https://www.amazon.com/SHIMANO-SH51-SPD-Cleat-Set/dp/B000R2MYB4>
- Basic Oxygen Furnace Steelmaking. (2019, August 28). Retrieved December 4, 2019, from <https://www.steel-technology.com/articles/oxygenfurnace>.
- Burke, E. (2003). High-tech Cycling. Human Kinetics.
- Catrike Boom Adjust Chain Tensioner – All Out Adventures. (2018, February 13). Retrieved from <https://alloutadventures.org/catrike-boom-adjust-chain-tensioner/>
- Catrike Expedition Recumbent Trike. (2015, January 27). Retrieved from <https://laidbackcycles.com/catrike-expedition-recumbent-trike/>
- Dual 120MM Cooling Fan. (n.d.). Retrieved December 4, 2019, from Computer Cable Store website: https://www.computercablestore.com/dual-120mm-cooling-fan?gclid=EAlaIQobChMI_MfcyKCd5gIVQtyGCh0h4QwrEAKYCCABEGJjOPD_BwE
- Eland, P. (n.d.). Tricycle steering geometry - the spreadsheets. Retrieved from http://www.eland.org.uk/steer_sheets.html
- EPA. nd. Energy and the environment. Retrieved from <https://www.epa.gov/energy/greenhouse-gases-equivalencies-calculator-calculations-and-references>.
- Fenner, P. (2010). On the Golden Rule of Trike Design.
- Fruehan, R.J., Fortini, O., Paxton, H.W., & Brindle, R. (2000). Theoretical Minimum Energies to Produce Steel for Selected Conditions. Retrieved from https://www.energy.gov/sites/prod/files/2013/11/f4/theoretical_minimum_energies.pdf.

Gregor, S. M., Perell, K. L., Rushatakankovit, S., Miyamoto, E., Muffoletto, R., & Gregor, R. J. (2002). Lower extremity general muscle moment patterns in healthy individuals during recumbent cycling. *Clinical Biomechanics*, 17(2), 123-129. doi:10.1016/s0268-0033(01)00112-7

Gulley, A. (2019, July 26). You Have No Excuse Not to Bike with a Light, Day or Night. Retrieved from <https://www.outsideonline.com/2064501/you-have-no-excuse-not-bike-light-day-or-night>

How to Build a Thermometer With Arduino UNO and the DS18B20 Waterproof Sensor | Arduino. (2018, September 13). Retrieved December 4, 2019, from Maker Pro website: <https://maker.pro/arduino/projects/how-to-build-a-thermometer-with-arduino-uno-and-the-ds18b20-waterproof-sensor>

LowCVP study highlights importance of measuring whole life carbon emissions. (2011, June 14). LowCVP. http://www.lowcvp.org.uk/news,lowcvp-study-highlights-importance-of-measuring-whole-life-carbon-emissions_1644.htm

NACA Duct. (n.d.). Retrieved December 4, 2019, from http://www.formula1-dictionary.net/naca_duct.html

Noraxon Wireless Surface EMG System. (2011, April 5). Use of Surface EMG in Sport Performance. Retrieved from <https://www.youtube.com/watch?v=u49aR1D8M40>

Power Grips. (2019). Retrieved from <http://powergrips.com>

SAS Output. (n.d.). Retrieved December 4, 2019, from https://www.eia.gov/electricity/annual/html/epa_a_03.html

Severy, D. M., Blaisdell, D. M., & Kerkhoff, J. F. (1976). AUTOMOTIVE SEAT DESIGN AND COLLISION PERFORMANCE. SAE Technical Paper Series. doi:10.4271/760810

Sheldon Brown's Bicycle Gear Calculator. (2019). Retrieved from <https://www.sheldonbrown.com/gear-calc.html>

Shennum, P. L., & deVries, H. A. (1976). The effect of saddle height on oxygen consumption during bicycle ergometer work. *Medicine and Science in Sports*, 8(2), 119–121.

Shigley, J. E. (2011). *Shigley's mechanical engineering design*. Tata McGraw-Hill Education.

Shimano XT CS-M8000 11 Speed Cassette. (2019, September 18). Retrieved from <https://www.jensonusa.com/Shimano-XT-CS-M8000-11-Speed-Cassette>

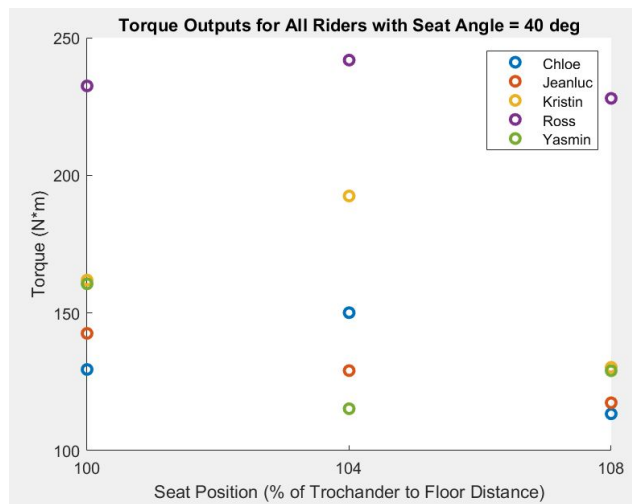
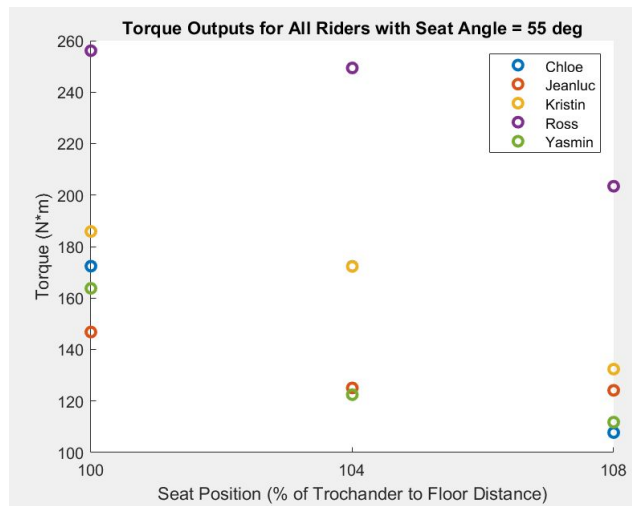
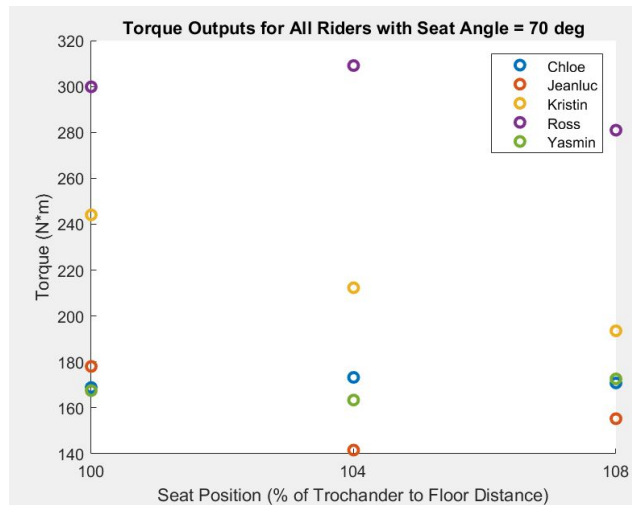
Shimano XT RD-M8000 11SP Rear Derailleur. (2017, April 4). Retrieved from <https://www.jensonusa.com/Shimano-XT-RD-M8000-11SP-Rear-Derailleur>

Stucky, A., Ward, R., Schrameyer, R., Sarosi, E., Sackandy, M., Weldon, K., Yoder, Z., Lynn, Z., Mitchell, R., Handerhan, S., Linderman, E., Hoydick, J. & Bartel, S. (2017). ASME human powered vehicle challenge. Retrieved from <https://www.dropbox.com/s/2jd5qjy04u4qzhf/2017-hpvc-east-design-22-UniversityOfPittsburgh.pdf?dl=0>.

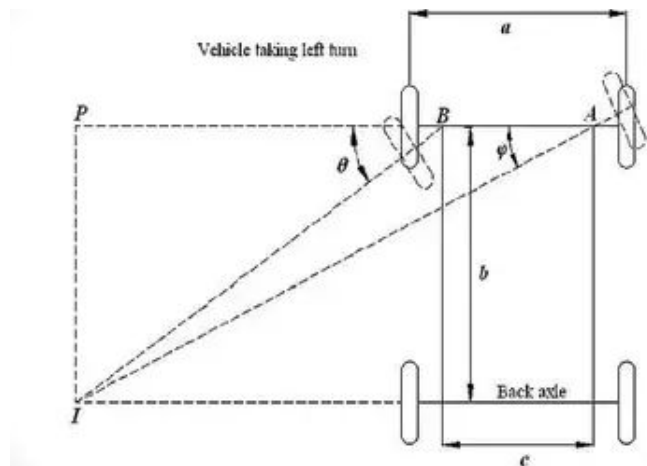
Tamai, G. (1999). The Leading Edge. Bentley Publishers.

7. Appendices

Appendix A: Biomechanics testing results



Appendix B: Steering Calculation Sheet for Turn Radius



a = wheel track

B = wheelbase

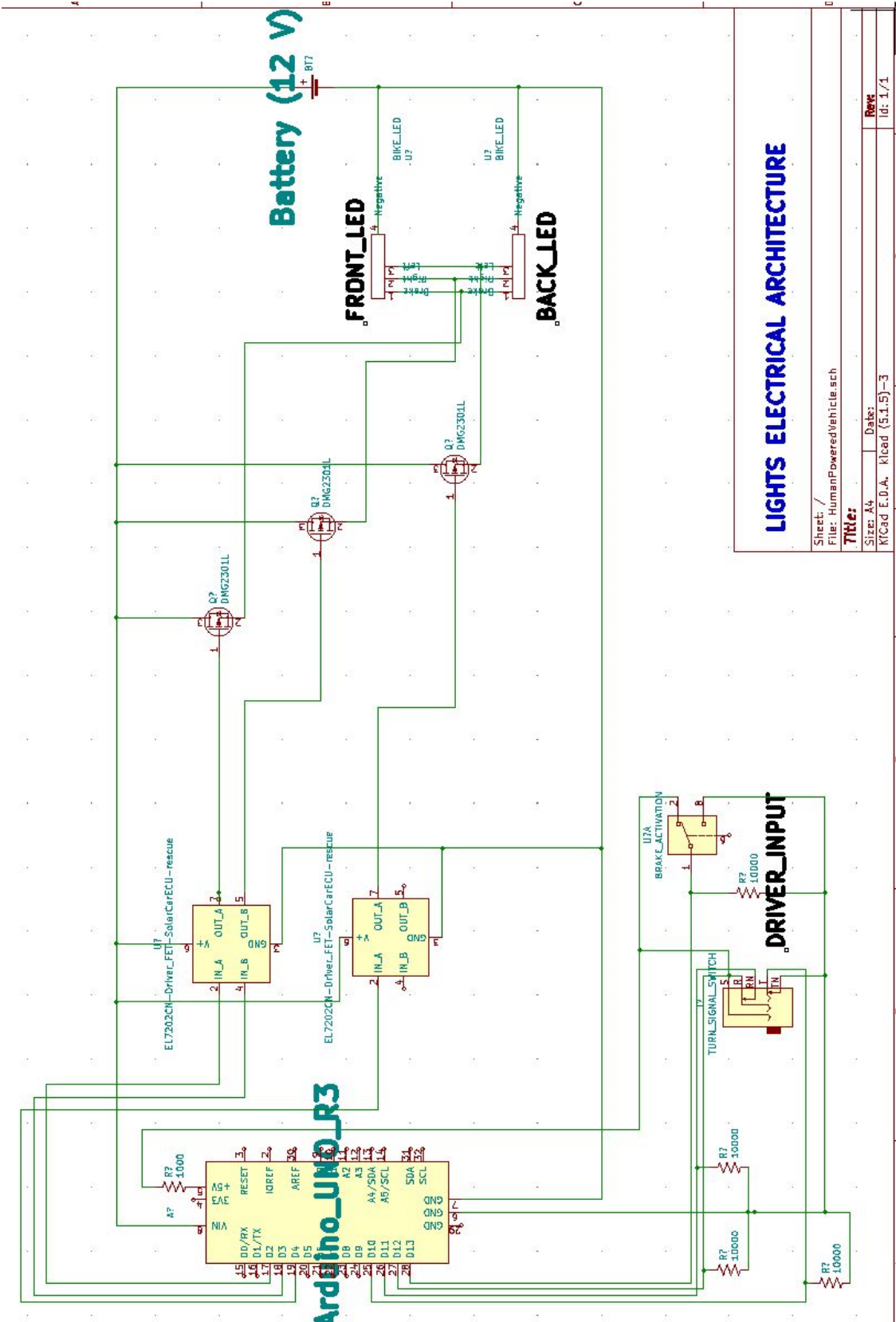
R = turning radius

Ψ = Angle of wheel compared to back wheel

$c = 0$

Figure for 2.5.5 turning radius

Appendix C: Vehicle Electrical Schematic for Turn Signals and Brake Lights



Appendix D: Itemized Cost Breakdown by Subteam

Subteam	Part Description	Unit Cost	Quantity	Total	Subteam	Part Description	Unit Cost	Quantity	Total
Frame	4130 Steel Pipe, 1.25" OD, 0.065" WT	\$60.89	4	\$243.56	Fairing	Plywood Boards	\$14.00	2	\$28.00
	4130 Steel Pipe, 1.00" OD, 0.065" WT	\$40.52	3	\$121.56		Garage Door Foam Board Insulation	\$23.00	16	\$368.00
	4130 Steel Pipe, 7/8" OD, 0.065" WT	\$38.15	2	\$76.30	Steering	Carbon fiber, 0.584" OD, 0.5" ID, 36" Length	\$83.80	1	\$83.80
	Front Wheel: Wheel Master Folding Bike Front Wheel - 20" x 1.5, Alloy, 36H, Black	\$42.55	2	\$85.10		4130 alloy steel 6*12*¼"	\$36.04	1	\$36.04
	Rear Wheel (Peloton)	\$62.99	1	\$62.99		6061 Aluminum sheet 3*6*¼"	\$38.74	1	\$38.74
	Tires, 27.5" DIA, Schwalbe Pro One (Peloton)	\$32.99	2	\$65.98		4130 Alloy Steel tube 7/8" OD, 0.805" ID, 3ft Length	\$21.57	1	\$21.57
	Tubeless Tire Sealant and Injector (Peloton)	\$10.79	1	\$10.79		0.827" ID, 4.921" Length	\$5.39	1	\$5.39
	Front Tires: Schwalbe Marathon 20*1.50'	\$31.14	3	\$93.42		Right-Hand ½"-20 Shank, Right-Hand Stud	\$190.20	1	\$190.20
Drivetrain	Rear Cassette: Shimano XT CS-M8000	\$82.08	1	\$82.08		Front and back aluminum alloy brakes with parking brake lock handle	\$44.94	1	\$44.94
	Rear Derailleur: Shimano XT M8000 Medium Cage	\$69.99	1	\$69.99	Innovation	LED Rear Light	\$9.95	2	\$19.90
	Chain Gobbler: Terracycle chain gobbler	\$155.11	1	\$155.11		Yellow LEDs, 5mm DIA	\$6.99	1	\$6.99
	Mesh Seat Fabric: Phifertex Fabric Mesh Samples	\$50.00	1	\$50.00		Electrical Wire	\$12.68	1	\$12.68
	Mesh Seat Straps: Plastic buckle, nylon strap	\$9.00	1	\$9.00		Arduino Uno R3	\$15.82	1	\$15.82
	Seat Cushion: Erg machine seat cushion	\$34.99	1	\$34.99		DS18B20 temperature probe	\$6.98	1	\$6.98
	Shifter: Bar end shifters (microshift BS-M11)	\$58.29	1	\$58.29		Dual 120mm Cooling Fans	\$22.09	1	\$22.09
	Shimano SPD cleats	\$11.74	4	\$46.96		NACA Duct	\$25.00	2	\$50.00
	Clipless Shoes	\$74.95	4	\$299.80		MOSFET Driver	\$1.74	2	\$3.48
	Shimano SPD pedals	\$61.44	1	\$61.44		P-Channel MOSFET	\$0.87	3	\$2.61
	Front Crankset 170mm Length, 38T	\$99.99	1	\$99.99		Buttons/Switches	\$10.00	1	\$10.00
	SHIMANO XT BB-MT800 BOTTOM BRACKET	\$19.99	1	\$19.99		Battery, 12V	\$33.99	1	\$33.99

	Chain Guards: Teflon tubing, 5'	\$7.00	1	\$7.00	Safety	Tanaka Phantom Safety Harness, 4 Point	\$63.88	1	\$63.88
	Standard bar tape (Peloton)	\$11.79	1	\$11.79		Horn	\$10.00	1	\$10.00
	Rear Tire Valve (Peloton)	\$7.99	1	\$7.99		Side View Mirror	\$7.00	2	\$14.00
	Rear Wheel Rim Tape (Peloton)	\$7.49	1	\$7.49	Tools	Tire Levers (Peloton)	\$2.69	1	\$2.69
	Chain: Peloton	\$48.00	1	\$48.00		Screwdrivers (Peloton)	\$10.89	1	\$10.89
	Power / Return Idler Wheel	\$106.00	2	\$212.00		Allen Wrenches (Peloton)	\$7.99	2	\$15.98
Fairing	Carbon Fiber	\$35.39	20	\$707.80		Chain Degreaser	\$14.95	1	\$14.95
	Epoxy	\$42.48	2	\$84.95		Chain Lube	\$8.99	1	\$8.99
	Resin	\$42.48	2	\$84.95	Total				\$4,065.91